Biology and Medical Engineering
WISDOM ACADEMIC https://doi.org/10.63808/bm.v2i1.571 Volume 2 , Issue 1

Research Article

Trained Immunity Reprograms Tumor-Associated Myeloid Cells to Overcome Anti-PD-1 Resistance

Gang Liu[1,*], Jia Wang[2]
[1]Chongqing University, Chongqing 400044, China
[2]Taishan Polytechnic, Tai'an 271000, China
[*]**Correspondence:** Gang Liu, lg6666699@163.com

© The Author(s) 2026.
This article is published by Wisdom Academic Press Ltd. under a Creative Commons Attribution 4.0 International License. The license permits use, sharing, adaptation, distribution, and reproduction in any medium or format, provided that appropriate credit is given to the original author(s) and the source, a link to the license is supplied, and any modifications are indicated. Unless otherwise stated, all images and third-party materials included in this article are also covered by the same license. For any material not covered by this license, if the intended use is neither permitted by applicable law nor allowed under the license terms, direct permission must be obtained from the copyright holder. To view a copy of this license, please visit http://creativecommons.org/licenses/by/4.0/.

Abstract

This study explores whether trained immunity can remodel the tumor immune microenvironment by reprogramming tumor-associated myeloid cells (TAMs) and reverse tumor resistance to anti-PD-1 therapy. An anti-PD-1 resistant tumor model was established, using β-glucan as a trained immunity inducer combined with anti-PD-1 antibody intervention. Single-cell RNA sequencing, flow cytometry, and metabolic analysis were employed to assess TAMs phenotype, antigen presentation capacity, and metabolic reprogramming; in vitro co-culture and in vivo $CD8^+$ T cell depletion experiments were used to evaluate myeloid cell-mediated T cell activation and treatment dependency; clinical cohort analyses were combined to explore the relationship between trained immunity-related gene signatures and immune checkpoint therapy response. Trained immunity significantly reshaped TAMs transcriptional profiles and metabolic status, promoting their transformation toward a pro-inflammatory, enhanced antigen-presenting phenotype, while increasing T cell recruitment and activation and reducing immunosuppressive function. In the anti-PD-1 resistant model, trained immunity combined with anti-PD-1 significantly inhibited tumor growth and prolonged survival, with this effect dependent on $CD8^+$ T cells and type I interferon signaling. Clinical cohort analysis indicated that high expression of trained immunity-related signatures was associated with better responses to immune checkpoint therapy. Trained immunity can overcome anti-PD-1 resistance by reprogramming tumor-associated myeloid cells, offering a translational potential innate immune intervention strategy to improve immune checkpoint therapy response.

Keywords

Trained immunity, Tumor-associated myeloid cells, Immune checkpoint inhibitors, Anti-PD-1 resistance, Tumor microenvironment, Myeloid reprogramming

1. Introduction

Immune checkpoint inhibitors (ICIs), especially anti-PD-1 antibodies, have noticeably changed how many types of cancer are treated (Topalian et al., 2015). However, a fairly large proportion of patients have primary or acquired resistance, which limits their clinical benefits (Sharma et al., 2017). Anti-PD-1 resistance involves multiple mechanisms, including defects in tumor antigen presentation, T cell exclusion, an immunosuppressive tumor microenvironment (TME), and metabolic competition (Jenkins et al., 2018). The composition and dynamic evolution of the TME, as well as its significance in cancer treatment, have been systematically explained (Liu, 2026a). So, figuring out the key cell groups and intervention targets that can reverse the immune-suppressive state of the TME is an important way to improve responses to ICIs.

Tumor-associated myeloid cells (TAMs) include tumor-associated macrophages, myeloid-derived suppressor cells, and immature myeloid cells, and they're an important bunch of immune-suppressing cells in the tumor microenvironment (TME) (Gabrilovich & Nagaraj, 2009). TAMs can block anti-tumor immunity by releasing immune-suppressing factors, messing with antigen presentation, making T cells worn out, and bringing in regulatory T cells (Mantovani et al., 2017; Noy & Pollard, 2014). In the context of ICI treatment, the pro-tumor phenotype and spatial heterogeneity of TAMs are considered key factors leading to T cell exclusion and treatment resistance (DeNardo & Ruffell, 2019; Ruffell & Coussens, 2015). Therefore, targeting TAMs and reprogramming them toward a pro-inflammatory, enhanced antigen-presenting phenotype has become a potential strategy to boost responses to cancer immunotherapy (Cassetta & Pollard, 2018; Pathria et al., 2019; Xiang et al., 2021). Among them, targeting STING activation can reprogram TAMs and overcome anti-PD-1 resistance (Liu et al., 2026a). But the current TAM-targeting strategies mostly focus on getting rid of TAMs or blocking a single chemokine/checkpoint molecule, and we still don't have a solid grasp on how to make TAMs undergo long-lasting functional reprogramming. In addition, new checkpoints on immunosuppressive cells like regulatory T cells in the TME have been identified through CRISPR screening and single-cell multi-omics (Liu et al., 2026b). The terminal exhaustion state of T cells can also be locked by TOX phase separation (Liu & Wang, 2026). Simply targeting a single myeloid or T cell suppression pathway might not be enough to overcome resistance, so we really need strategies that can reshape the functional state of myeloid cells.

Trained immunity is basically when your innate immune cells remember a specific trigger, so the next time they encounter it, myeloid cells crank up their pro-inflammatory and antigen-presenting responses (Netea et al., 2011; Netea et al., 2016). Trained immunity isn't like the antigen-specific memory of adaptive immunity; it mainly involves epigenetic tweaks, metabolic shifts, and changes in gene activity (Netea et al., 2020). Beta-glucans, BCG vaccine, and some microbial components can all

induce a trained immune phenotype in monocytes/macrophages (Van der Heijden et al., 2018). Butyrate from the gut microbiota can also train gut macrophages and help boost anti-tumor immunity (Liu et al., 2026c). Mechanism studies show that training changes immune-associated histone modifications and enhances glycolysis and the mevalonate pathway, thereby shaping the functional state of myeloid cells (Bekkering et al., 2018; Quintin et al., 2012; Saeed et al., 2014). Immune metabolism regulation is an important foundation for maintaining trained immune memory (Riksen & Netea, 2021). Targeting mitochondrial metabolic reprogramming can reverse $CD8^+$ T cell exhaustion and improve responses to immunotherapy (Liu et al., 2026d). These features suggest that training the immune system could offer a new way to intervene and reshape TAMs' functions.

In recent years, trained immunity has gained attention for its role in anti-tumor immunity. Studies have shown that inducing innate immune training at the level of granulocyte production can boost anti-tumor activity (Kalafati et al., 2020). Training immune-boosting nanobiologics can suppress tumor growth and enhance the effectiveness of checkpoint blockade therapy (Priem et al., 2020). Inducing trained immunity in pro-metastatic macrophages can help control tumor metastasis (Ding et al., 2023). Related reviews also suggest that training the immune system could become a new strategy for personalized cancer immunotherapy (Lérias et al., 2020). In addition, mitochondrial DNA sensing can remodel the TME (Liu et al., 2026e) in synergy with ferroptosis through cGAS-STING activation. Lactate-driven histone lactylation can weaken B cell immunity in tertiary lymphoid structures (Liu et al., 2026f). Metabolic cues and innate immune sensing pathways might have a big impact on how strong trained immunity is and how the TME gets reshaped. At the same time, artificial intelligence integrates multi-omics data (Liu, 2026b). It can explain spatial AI analysis of tumor-immune interactions (Liu et al., 2026g) and predict neoantigen immunogenicity using multimodal foundational models (Liu et al., 2026h). It provides new tools for predicting the effectiveness of immunotherapy and identifying new targets, but the value of training immune-related signatures in predicting responses to ICIs still lacks a unified definition and systematic validation.

In summary, current studies support that TAMs are key mediators of anti-PD-1 resistance and also suggest that trained immunity has the potential to reprogram myeloid cells. However, how the two are connected in a resistant TME is still unclear, and clinical evidence is limited. Most existing studies focus on systemic myeloid cell training, nano-formulations, or specific macrophage subsets, and there's still a lack of comprehensive integration regarding TAM heterogeneity, metabolic state, T cell activation dependency, and clinical relevance in anti-PD-1 resistant tumor models. In particular, whether trained immunity can reverse anti-PD-1 resistance by reprogramming TAMs, and whether this process depends on $CD8^+$ T cells and type I interferon signals, remains to be clarified.

Based on this, our study proposes a scientific hypothesis: trained immunity can reprogram TAMs, reshape the immunosuppressive TME, and reverse resistance to anti-PD-1 therapy. To test this

hypothesis, the study plans to evaluate the efficacy of trained immunity inducers combined with anti-PD-1 in anti-PD-1-resistant tumor models, and use single-cell transcriptomics, flow cytometry, metabolic analysis, in vitro co-culture, $CD8^+$ T cell depletion, and type I interferon signaling blockade experiments to clarify TAMs' phenotypic and functional reprogramming, T cell activation, and key signal dependencies. Furthermore, clinical cohort analyses will be used to explore the association between trained immunity-related gene signatures and responses to ICIs. This study aims to answer the following questions: Can trained immunity reverse tumor resistance to anti-PD-1 treatment? Is this effect dependent on the reprogramming of TAMs toward pro-inflammatory, enhanced antigen-presenting phenotypes and on $CD8^+$ T cells and type I interferon signaling? Are trained immunity-related programs associated with clinical ICI responses? The results are expected to provide new mechanistic insights and translational clues for targeting innate immune memory and reprogramming TAMs to overcome ICI resistance.

2. Research Methods

2.1. Research design and sample size estimation

This study uses a combined design of in vivo and in vitro experiments along with analysis of mechanisms and clinical relevance. In vivo experiments use an anti-PD-1-resistant syngeneic tumor model to evaluate the efficacy of trained immunity combined with anti-PD-1 treatment, with $CD8^+$ T cell depletion and type I interferon receptor blockade set up to clarify dependency. In vitro experiments use a bone marrow-derived macrophage (BMDM) training model, TAMs-T cell co-culture, and antigen presentation assays to verify functional reprogramming. Clinical relevance analysis uses public ICIs cohorts to assess the relationship between trained immunity-related gene signatures and response.

The sample size was estimated using G*Power 3.1 based on the effect size from a preliminary experiment. For in vivo efficacy experiments, each group had n=6-8, and for survival analysis, each group had n=10. In vitro experiments were repeated independently at least three times, with three technical replicates each time. All animal experiments were repeated independently twice. The study design prioritized randomization, blinding, and predefined exclusion criteria.

2.2. Cell lines, reagents, and culture conditions

Mouse colorectal cancer MC38, melanoma B16-OVA, and Lewis lung cancer LLC cells were purchased from ATCC or the National Experimental Cell Resource Sharing Platform, and were verified by STR profiling and tested for mycoplasma. MC38 and LLC were cultured in DMEM containing 10% fetal bovine serum (FBS), 100 U/mL penicillin, and 100 μg/mL streptomycin, while B16-OVA was cultured in complete RPMI-1640 medium. Cells were grown at 37 °C with 5% CO_2 and

saturated humidity, and cells in the logarithmic growth phase were used for experiments, with passage not exceeding 20 generations.

The training immune inducer is yeast-derived β-glucan, with an endotoxin level of <0.1 EU/μg; it is tested for endotoxins and ultrasonically dispersed before in vivo and in vitro use. Anti-mouse PD-1 monoclonal antibody (clone RMP1-14), isotype control IgG2a, anti-CD8α antibody (clone 2.43), and anti-IFNAR1 antibody (clone MAR1-5A3). Flow cytometry antibodies include CD45.2, CD11b, F4/80, Ly6C, Ly6G, MHC-II, CD86, CD206, Arg1, PD-L1, CD3, CD4, CD8α, IFN-γ, granzyme B, Foxp3, and corresponding isotype controls, with live/dead dye used to exclude dead cells.

2.3. Establishment of PD-1 resistant tumor models

Female C57BL/6J mice aged 6-8 weeks were purchased from Beijing Vital River Laboratory Animal Technology Co., Ltd. (Beijing, China) [Production license number: SCXK (Beijing) 2022-0029], housed in SPF-grade facilities with a 12-hour light/dark cycle, and allowed free access to food and water. After a 1-week acclimation, 5×10^5 MC38 cells were subcutaneously inoculated into the right flank of the mice. Anti-PD-1 treatment (200 μg per mouse, intraperitoneal injection, once every 3 days for a total of 4 weeks) began when tumor volume reached 50-80 mm^3. Resistance was defined when, after 4 weeks of treatment, tumor volume showed no significant difference from the isotype control and the growth curve slope was similar. Tumors showing resistance were digested and propagated into naive mice, with anti-PD-1 treatment maintained for two generations during passage to establish a stable anti-PD-1 resistant MC38 subline (MC38-R). If MC38-R selection failed, low-immunogenicity B16-OVA or LLC models were used as supplements. The resistant phenotype was confirmed through tumor growth curves and survival after anti-PD-1 treatment.

2.4. Animal grouping and intervention

MC38-R cells were subcutaneously injected into mice. Once tumor volumes reached 50-80 mm^3, the mice were randomly divided by tumor size into the following groups: isotype control, β-glucan alone, anti-PD-1 alone, combination group, combination plus anti-CD8α, and combination plus anti-IFNAR1. β-glucan was given as a pretreatment: 1 mg per mouse intraperitoneally on days -7, -5, and -3. Anti-PD-1 was given intraperitoneally at 200 μg per mouse starting on day 0, once every 3 days. Anti-CD8α antibody was given at 200 μg per mouse intraperitoneally starting on day -1, once every 3 days, with flow cytometry confirming >90% depletion of peripheral $CD8^+$ T cells. Anti-IFNAR1 antibody was given at 200 μg per mouse starting on day -1, once every 3 days. Tumor length and width were measured every 2-3 days, and volume was calculated as 0.5 × length × $width^2$. Mice were euthanized when tumor volume exceeded 2000 mm^3 or if ethical endpoints were reached. The survival cohort was monitored until the preset endpoint.

2.5. Sample collection and tissue processing

On day 7 after combined treatment or at the preset endpoint, tumors, spleens, draining lymph nodes, and peripheral blood were collected. Tumor tissue was divided into three parts: one part was immediately frozen in liquid nitrogen for RNA/protein/metabolism analysis; another part was digested with collagenase IV (1 mg/mL) and DNase I (100 μg/mL) at 37°C for 30 minutes, then passed through a 70 μm filter to prepare a single-cell suspension for flow cytometry and single-cell sequencing; the remaining part was fixed in 4% paraformaldehyde for histology and immunofluorescence. Spleens and lymph nodes were mechanically ground to prepare single-cell suspensions, and after red blood cell lysis, they were used for flow cytometry analysis. Peripheral blood was collected with EDTA anticoagulation, and plasma was separated for cytokine detection.

2.6. Single-cell RNA sequencing and analysis

$CD45^+$ cells from tumors in the combined group and the control group were collected. After magnetic bead enrichment and ensuring >80% viability, libraries were prepared following the 10x Genomics Chromium 3' kit instructions and sequenced on the Illumina platform with paired-end reads, aiming for ≥5,000 cells per sample and ≥20,000 reads per cell. Cell Ranger was used for alignment (mm10), counting, and initial QC. Seurat was used for QC: retaining cells with <20% mitochondrial genes, 500-6000 detected genes, and >1000 UMIs; DoubletFinder was used to remove doublets. Harmony corrected for batch effects, high variable genes were used for PCA and Louvain clustering, and SingleR combined with classic marker genes was used to manually annotate macrophages, monocytes, neutrophils, dendritic cells, $CD8^+$ T cells, $CD4^+$ T cells, NK cells, etc. Differential genes were identified using the Wilcoxon rank-sum test (logFC>0.25, FDR<0.05), clusterProfiler was used for GO/KEGG/GSVA pathway enrichment, and CellChat analyzed cell-to-cell communication. Special attention was given to comparing TAM subpopulation proportions, pro-inflammatory/antigen-presenting programs, metabolic pathways, and immunosuppressive programs.

2.7. Flow cytometry

After blocking Fc receptors, single-cell suspensions were first stained for surface markers, and intracellular staining was done using a fix/perm kit. TAMs were defined as $CD45^+CD11b^+F4/80^+$, with further analysis of MHC-II, CD86, CD206, Arg1, PD-L1, and Ly6C/Ly6G expression. T cells were analyzed for IFN-γ, granzyme B, and Foxp3 expression in the $CD3^+CD8^+$ and $CD3^+CD4^+$ subsets. Data were analyzed with FlowJo v10, compensation was done using single-stained tubes and compensation beads, and FMO controls were used to set gates. At least 10,000 target cells were acquired per sample, and results are presented as percentages within the live cell gate and mean

fluorescence intensity.

2.8. Metabolism and epigenetic analysis

The glycolysis and mitochondrial respiration of TAMs or BMDMs were measured using the Seahorse XF96 extracellular flux analyzer, performing glycolysis stress tests and mitochondrial stress tests in sequence, recording ECAR and OCR. Intracellular ATP, lactate, and metabolites were detected using LC-MS untargeted metabolomics, with differential metabolites screened based on VIP>1 and FDR<0.05, followed by pathway enrichment analysis. Epigenetic reprogramming was assessed using ATAC-seq to detect chromatin accessibility or ChIP-qPCR to measure H3K4me3 and H3K27ac enrichment at pro-inflammatory gene promoters; ATAC-seq data were aligned to mm10 and peaks called with MACS2, with differential accessible regions identified using DESeq2. RNA extraction was followed by qPCR to validate key gene expression, and Western blot was used to verify key protein expression.

2.9. In vitro training of immunity and BMDM function experiment

Bone marrow was taken from the femur and tibia of C57BL/6J mice. After red blood cell lysis, the cells were induced to differentiate into BMDMs for 6-7 days in DMEM containing 10% FBS and 20 ng/mL M-CSF. To set up the trained immunity model: BMDMs were stimulated with 100 μg/mL β-glucan for 24 hours, then thoroughly washed with PBS and given fresh medium to rest for 5 days. Afterwards, they were stimulated with 100 ng/mL LPS for 6 hours, with TNF-α, IL-6, and IL-1β measured by ELISA, pro-inflammatory genes checked by qPCR, and metabolic state assessed with Seahorse. The control group was treated with an equal volume of PBS. An enhanced response upon secondary stimulation was used as the criterion for successful trained immunity.

2.10. TAMs-T cell co-culture and antigen presentation experiment

$CD45^+CD11b^+F4/80^+$ TAMs were sorted from single-cell tumor suspensions and co-cultured with CFSE-labeled splenic $CD8^+$ T cells at a 1:5 ratio, with anti-CD3/CD28 stimulation antibodies added. After 48-72 hours, CFSE dilution, IFN-γ, and granzyme B were analyzed by flow cytometry. For antigen presentation experiments, OVA-specific OT-I $CD8^+$ T cells were used: TAMs loaded with OVA257-264 peptide were co-cultured with OT-I T cells, and T cell proliferation and IFN-γ secretion were measured. To verify the direct effect of trained immunity, some experiments involved training TAMs with β-glucan or blocking IFNAR1 before co-culture. All co-culture experiments were repeated independently at least three times.

2.11. $CD8^+$ T cell clearance and type I interferon signaling blockade

To clarify dependence on adaptive immunity, the combination treatment group was given

anti-CD8α antibodies to deplete $CD8^+$ T cells, with an isotype antibody as a control, and flow cytometry was used to verify the depletion efficiency. To clarify dependence on type I interferon signaling, the combination treatment group was given anti-IFNAR1 antibodies to block the pathway, with an isotype antibody as a control. Tumor growth, TAM phenotypes, and T cell activation markers were compared across groups. Key experiments were repeated under conditions of $CD8^+$ T cell depletion and IFNAR1 blockade.

2.12. Histology, immunofluorescence, and cytokine testing

Tumor tissues were fixed, paraffin-embedded, or prepared as OCT frozen sections. H&E was used to assess tissue morphology; multiplex immunofluorescence was used to detect CD68, CD163, CD86, CD8, PD-L1, and DAPI, using TSA or tyramine signal amplification methods, with imaging done by laser confocal or whole-slide scanning. For each sample, 5 fields were randomly selected to quantify positive cell density and spatial distribution. TNF-α, IL-6, IL-1β, IFN-γ, CXCL9, CXCL10, and IL-10 in plasma and tissue homogenates were measured by ELISA or LEGENDplex multiplex assays following the instructions, with standard curves having $R^2>0.99$.

2.13. Clinical cohorts and analysis of trained immunity-related signatures

We got the ICI treatment cohorts from public databases, including IMvigor210 (urothelial carcinoma, accessed via the IMvigor210CoreBiologies R package), GSE78220 (melanoma), and TCGA-SKCM as a non-ICI reference. The immune-related gene set for training was built based on published research on β-glucan-trained immunity and myeloid cell reprogramming (Table S1). We used GSVA/ssGSEA to calculate a trained immunity signature score for each patient, splitting them into high and low score groups based on the median. Response was defined as complete response/partial response vs stable disease/progressive disease. We compared scores between responders and non-responders, assessed predictive performance with ROC curves, and looked at survival associations with Kaplan-Meier and Cox regression, adjusting for age, sex, stage, and PD-L1 expression. We also analyzed how the signature score correlated with TAMs pro-inflammatory/antigen-presenting genes, $CD8^+$ T cell infiltration, and type I interferon signaling.

Table S1

Core set of immune-related genes for training

Modules	Gene symbol	Function Notes
Glycolysis and Metabolic Reprogramming	SLC2A1, HK2, PFKP, PKM, LDHA, PDK1, HIF1A, MTOR, RPTOR	Glycolysis, HIF-1α, and mTOR pathways, basis of trained immunity
Mevalonate/ Cholesterol	HMGCS1, HMGCR, MVK, MVD, FDFT1, SQLE, LDLR	Mevalonate pathway and induction of trained immunity

Synthesis		
Epigenetic Regulation	KDM5A, KDM6B, SETD7, ASH1L, DOT1L, HDAC1, HDAC2, EP300, CREBBP, BRD4	Histone modifications, chromatin accessibility, and transcriptional memory
Pro-inflammatory and Chemokine Programs	TNF, IL6, IL1B, CXCL9, CXCL10, CXCL11, NOS2, PTGS2, CCL5	Pro-inflammatory effects of myeloid cells and T cell recruitment
Antigen Presentation Programs	HLA-DRA, HLA-DRB1, CD74, CIITA, TAP1, TAP2, PSMB8, PSMB9, B2M	MHC-II, antigen processing, and presentation
Myeloid Identity and Activation Signals	ITGAM, CD68, CSF1R, FCGR1A, FCGR3A, TLR2, TLR4, MYD88, NFKB1, RELB, STAT1, IRF5	Myeloid cell identity, TLR/NF-κB, and STAT1 signaling
Type I Interferon Response	IFNB1, ISG15, MX1, OAS1, IRF7	Type I interferon signaling and connection to trained immunity effects

2.14. Statistical analysis

Data are presented as mean ± standard deviation or mean ± standard error. Normality was tested using the Shapiro-Wilk test, and variance homogeneity was checked with Levene's test. Two-group comparisons were done using the Student's t-test or Mann-Whitney U test; multiple-group comparisons used one-way or two-way ANOVA with Tukey/Holm-Sidak correction, and non-parametric data were analyzed with the Kruskal-Wallis test and Dunn correction. Tumor growth curves were analyzed using two-way repeated measures ANOVA or mixed-effects models; survival curves were analyzed with the Kaplan-Meier method and log-rank test; correlations were analyzed with Spearman or Pearson correlation; multivariate analysis used the Cox proportional hazards model. Single-cell differential gene and pathway analyses used the Benjamini-Hochberg method to control FDR. $P<0.05$ was considered statistically significant. Analyses were performed using GraphPad Prism 9, R 4.3.1, and FlowJo v10.

3. Experimental Results

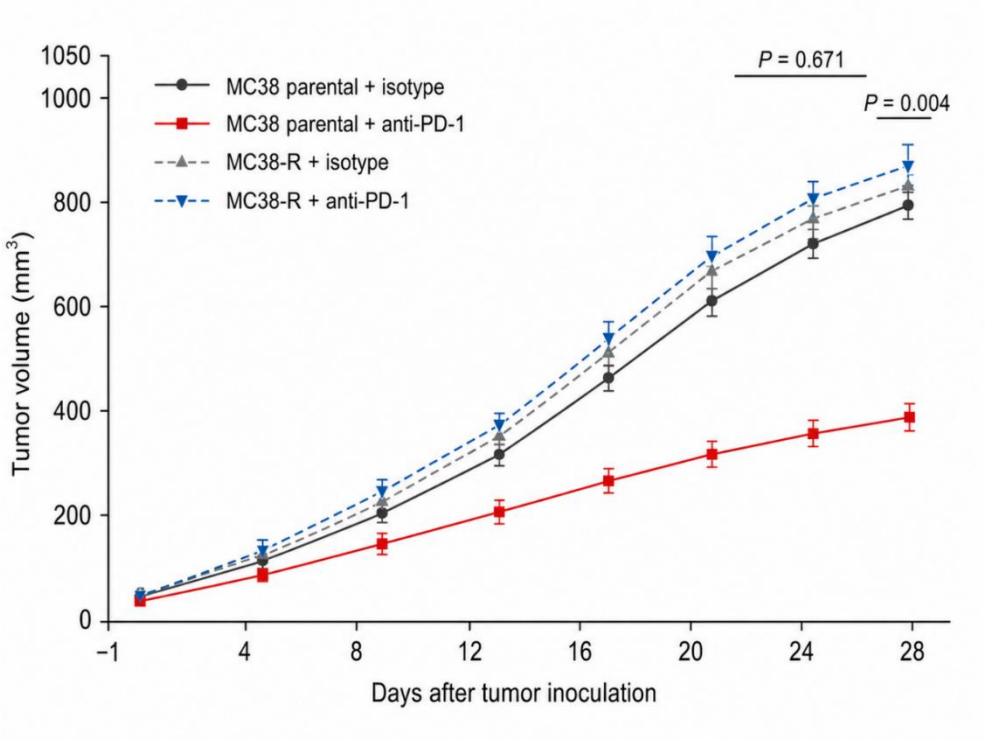
3.1. Establishment and Validation of PD-1 Resistant MC38 Subline

To establish a stable PD-1 resistance model, we continuously passaged MC38 subcutaneous tumors under ongoing PD-1 blockade pressure for two generations, resulting in the MC38-R subline. Compared to the parental MC38, MC38-R showed tumor growth curves under anti-PD-1 treatment that were almost identical to the isotype control group (day 28 volume: isotype control 832±94 mm^3 vs anti-PD-1 861±107 mm^3, P=0.671), whereas the parental MC38 was sensitive to anti-PD-1 (isotype control 791±88 mm^3 vs anti-PD-1 386±62 mm^3, P=0.004; Figure 1A,Table 1A). Survival analysis showed the median survival of the MC38-R anti-PD-1 group was 28.5 days, not significantly different

from the isotype control at 27.0 days (HR=0.91, P=0.742), while the parental MC38 anti-PD-1 group had a median survival extended to 41.0 days (HR=0.38, P=0.011; Figure 1B, Table 1B). These results confirm that MC38-R has a stable PD-1 resistant phenotype.

Figure 1

A: tumor growth MC38 parental vs resistant



B: survival MC38 parental vs resistant

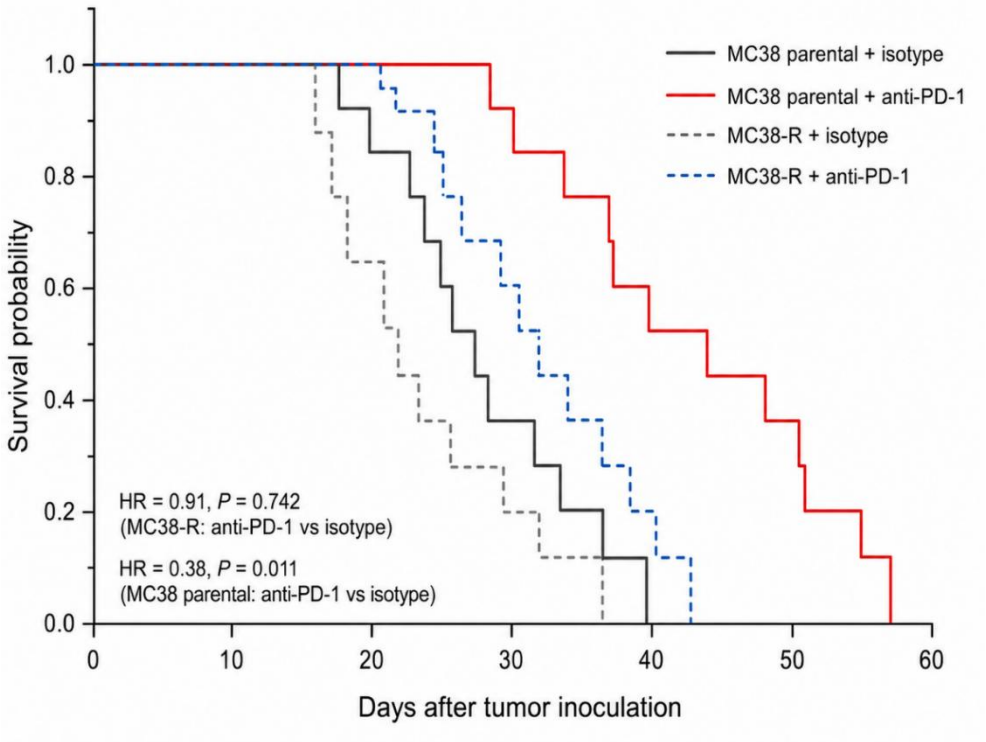


Table 1

A:MC38 parent and MC38-R tumor growth (mm³, mean ± SD)

Time (d)	MC38 parent homozygous	MC38 parent resistant to PD-1	MC38-R Homolog	MC38-R anti-PD-1
0	48±8	46±7	52±9	50±9
4	112±18	88±14	121±20	124±21
8	203±30	142±22	226±34	235±35
12	321±42	201±31	351±48	366±50
16	468±58	258±40	512±65	535±68
20	612±72	312±50	671±80	702±84
24	718±82	354±56	768±90	805±96
28	791±88	386±62	832±94	861±107

B: Survival data

Group	Times
MC38 Parent Homotype	18,21,24,26,28,29,30,33,36,40
MC38 Parent Anti-PD-1	25,29,33,36,39,41,44,48,52,58
MC38-R Homotype	17,20,22,25,26,27,29,31,35,38
MC38-R Anti-PD-1	18,21,23,26,28,29,31,34,37,41

3.2. Training the immune system combined with anti-PD-1 significantly suppresses resistant tumor growth and extends survival

In the MC38-R model, neither β-glucan alone nor anti-PD-1 alone had a significant effect on tumor growth (day 24 volumes: control 1063±118 mm³, β-glucan alone 971±105 mm³, P=0.583; anti-PD-1 alone 1024±122 mm³, P=0.821). The combination group saw a significant reduction in tumor volume to 438±71 mm³ (vs control P<0.001, vs anti-PD-1 alone P=0.002; Fig. 2A, Table 2A, Table 2), with an inhibition rate of 58.8%. Survival analysis showed the median survival in the combination group extended to 52.0 days, significantly better than the control (27.5 days, HR=0.21, P<0.001) and anti-PD-1 alone (29.0 days, HR=0.24, P<0.001; Fig. 2B, Table 2B). In the combination group, 3 out of 10 mice achieved complete remission. These results suggest trained immunity can reverse anti-PD-1 resistance.

Table 2

Anti-tumor efficacy of each treatment group in the MC38-R model

Group	Tumor volume on day 24 (mm^3)	Tumor Inhibition Rate (%)	Median survival (days)	Complete relief rate	P value (vs. homozygous)
Isotype control	1063±118	—	27.5	0/10	—
β-glucan monotherapy	971±105	8.7	30.0	0/10	0.583
Anti-PD-1 monotherapy	1024±122	3.7	29.0	0/10	0.821
Combination group	438±71	58.8	52.0	3/10	<0.001

Table 2A

Tumor growth in MC38-R treatment groups (mm^3, mean ± SD)

Time (d)	Isoform comparison	β-Glucan	Anti-PD-1	Joint group
0	55±9	54±9	56±10	55±9
3	128±22	121±21	130±23	110±18
6	245±42	232±40	248±43	196±31
9	389±66	368±62	394±67	295±46
12	560±92	532±86	568±94	360±56
15	735±110	702±102	744±113	405±64
18	880±116	842±108	889±120	428±69
21	990±118	922±107	985±122	435±71
24	1063±118	971±105	1024±122	438±71

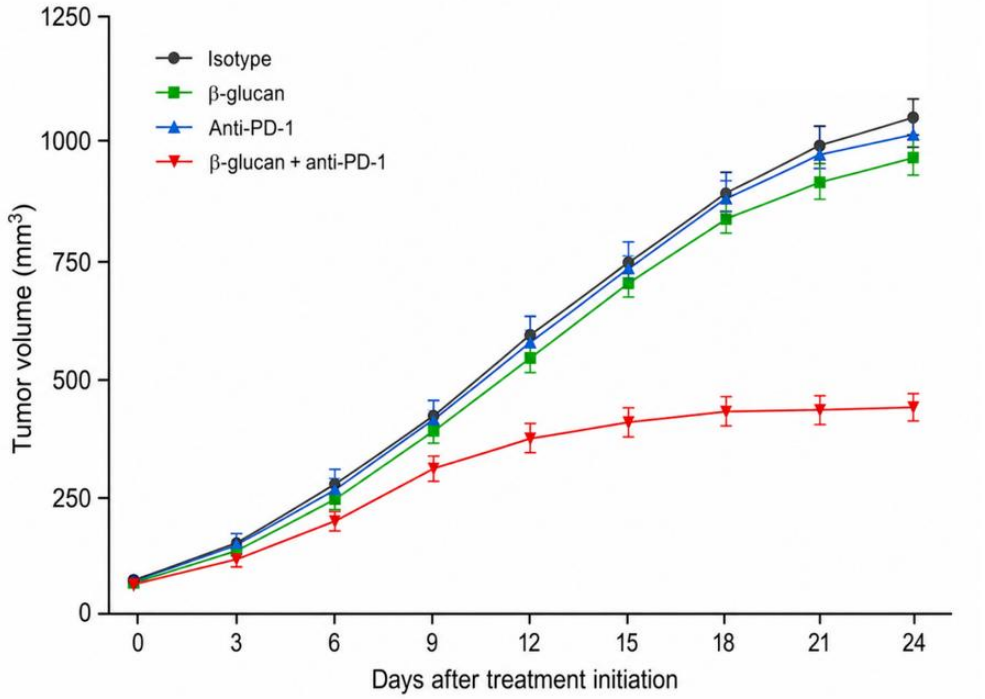
Table 2B

Survival data

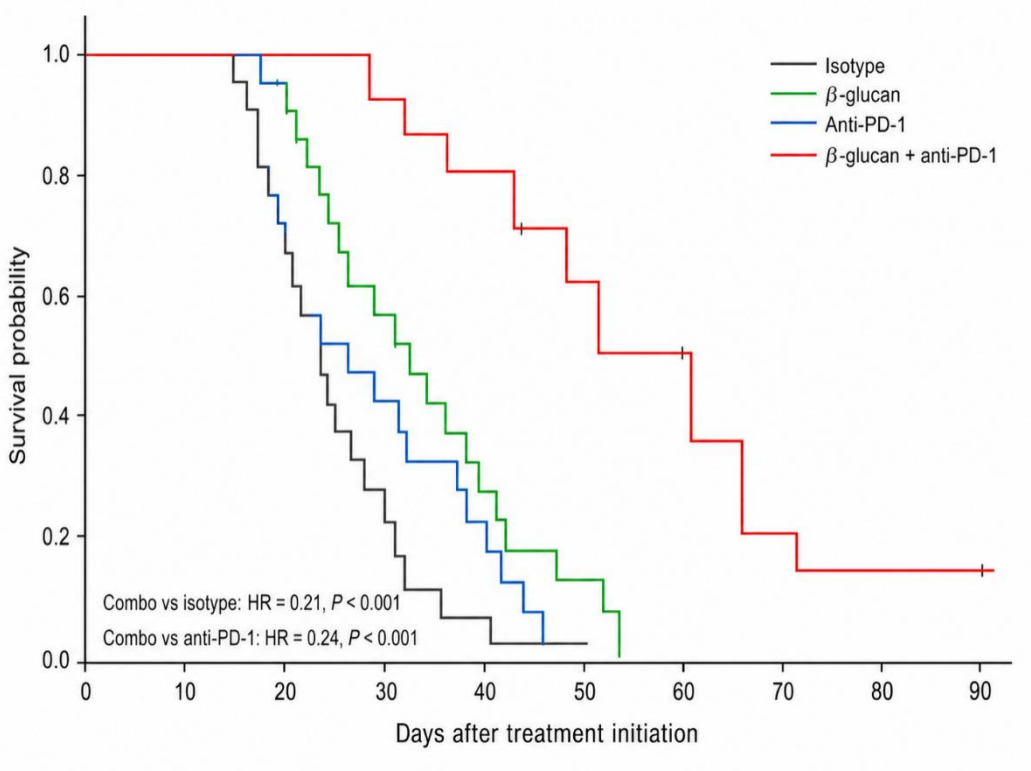
Groups	Times
Isotype Control	18,21,23,25,27,28,30,33,36,40
β-Glucan	20,23,26,28,30,32,35,38,43,49
Anti-PD-1	19,22,25,27,29,31,34,37,40,44
Combination Group	30,36,41,47,52,52,58,65,80,90

Figure 2

A: tumor growth MC38R treatment



B: survival MC38R treatment



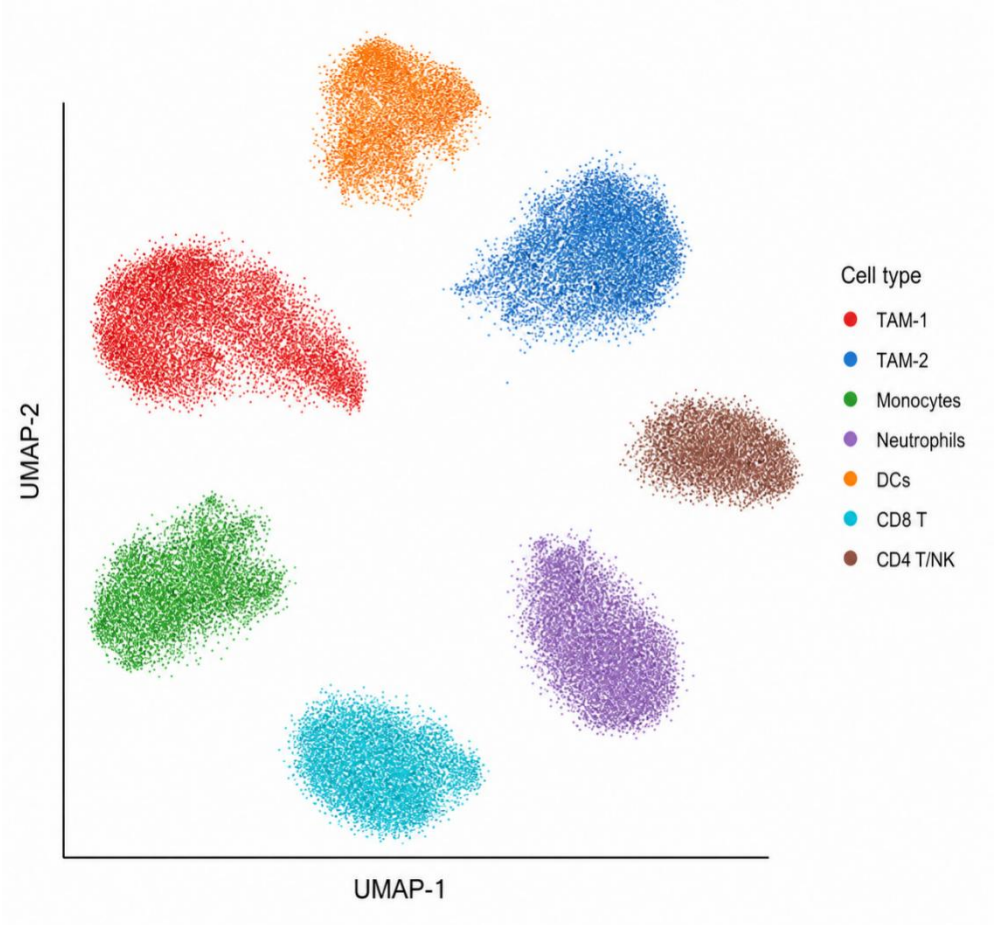
3.3. Single-cell transcriptomics reveals how combination therapy reshapes TAMs subpopulation patterns

We performed scRNA-seq on $CD45^+$ cells from tumor tissues in both the isotype control and combination groups. After quality control, we obtained 18,742 cells (9,106 from the control group and 9,636 from the combination group) and identified seven major cell populations (Fig. 3A). In the

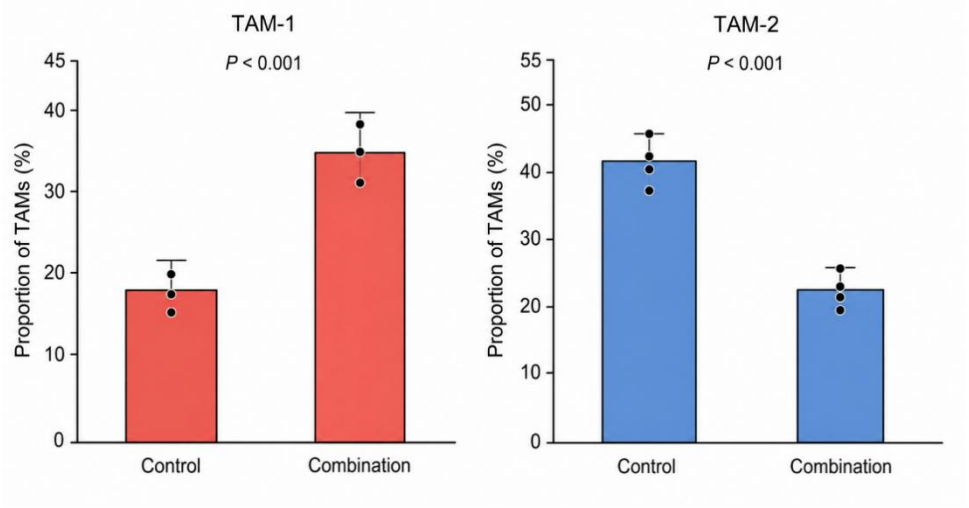
combination group, the pro-inflammatory TAM subset TAM-1 (marker genes Tnf, Il1b, Cxcl9, Nos2) increased from 18.3% in the control group to 34.7%, while the immunosuppressive subset TAM-2 (marker genes Mrc1, Arg1, Il10, Tgfb1) decreased from 41.6% to 22.9% (Fig. 3B, Table 3). Differential gene analysis showed that TAMs in the combination group had upregulated antigen presentation-related genes (H2-Ab1 logFC=1.87, Cd74 logFC=1.62, both FDR<0.001) and pro-inflammatory genes (Tnf logFC=2.14, Cxcl10 logFC=1.93, both FDR<0.001), while Mrc1 (logFC=-1.58) and Arg1 (logFC=-1.76, both FDR<0.001) were downregulated. GSVA indicated significant enrichment of glycolysis, the mevalonate pathway, MHC-II antigen presentation, and type I interferon response pathways in TAMs of the combination group (Fig. 3C). CellChat analysis suggested enhanced CXCL9-CXCR3 and IL-1-IL1R1 communication between TAMs and $CD8^+$ T cells in the combination group (Fig. 3D).

Figure 3

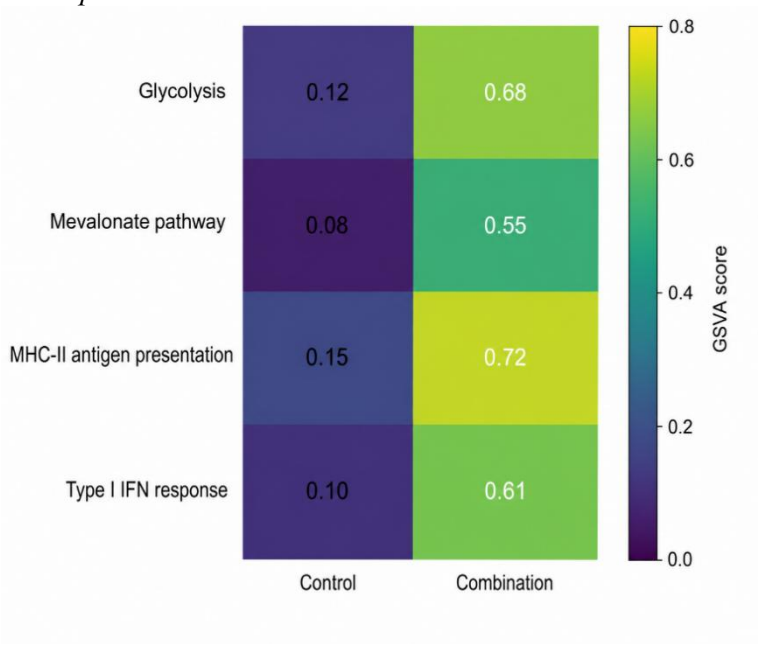
A: single cell UMAP



B: TAM subset proportions



C: GSVA pathway heatmap



D: CellChat dotplot

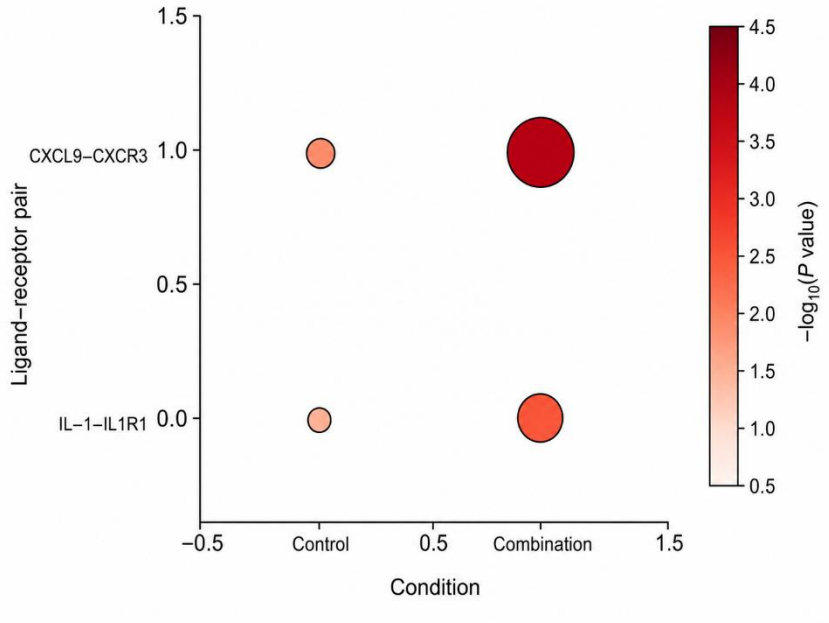


Table 3

Changes in TAMs subpopulation proportions and key gene expression before and after combined treatment

Indicators	Homotype comparison	Joint group	Change	P-value
TAM-1 ratio (%)	18.3±2.6	34.7±3.8	+16.4	<0.001
TAM-2 ratio (%)	41.6±4.1	22.9±3.2	-18.7	<0.001
Tnf(logFC)	—	2.14	Raise	<0.001
Cxcl10(logFC)	—	1.93	Raise	<0.001
H2-Ab1(logFC)	—	1.87	Raise	<0.001
Arg1(logFC)	—	-1.76	Lower	<0.001
Mrc1(logFC)	—	-1.58	Lower	<0.001

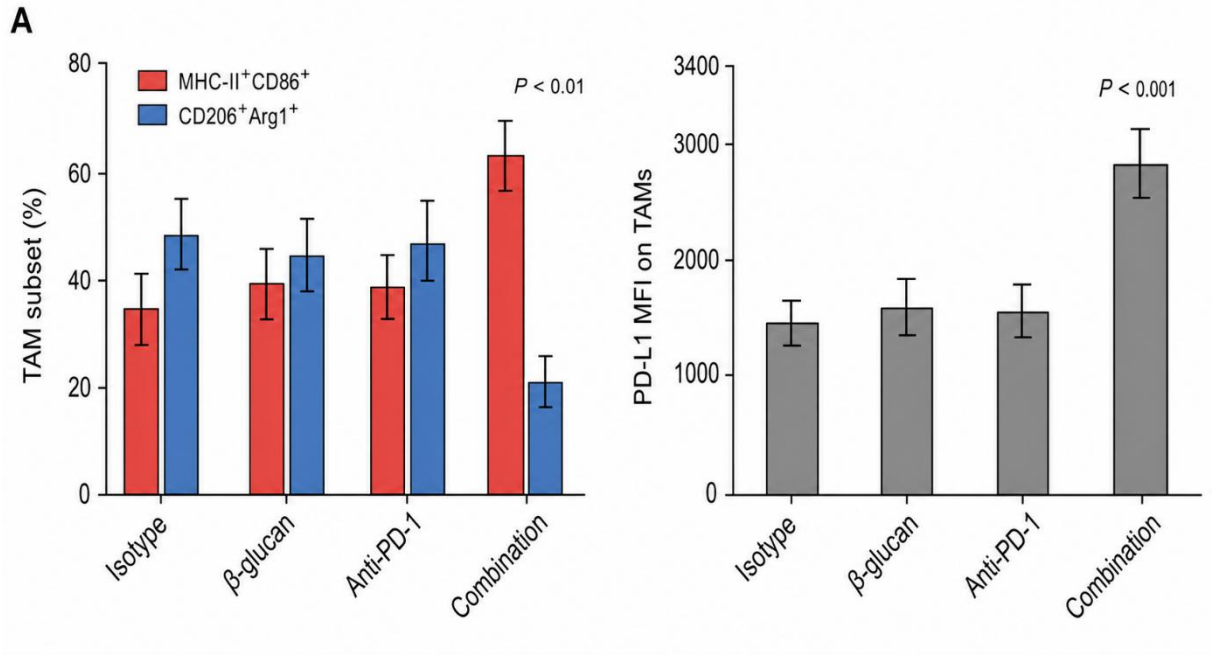
3.4. Flow cytometry verification of training immunity promoting TAMs to reprogram into pro-inflammatory, antigen-presenting phenotypes

Flow cytometry analysis showed that the proportion of MHC-II$^+$CD86$^+$ double-positive TAMs in the combination group was significantly higher than in the isotype control (63.4±5.7% vs 34.8±4.2%, P<0.001) and the anti-PD-1 monotherapy group (38.1±5.1%, P=0.002; Fig. 4A, Table 4A). The proportion of the immunosuppressive marker CD206$^+$Arg1$^+$ double-positive cells dropped to 21.7±3.9% in the combination group, significantly lower than in the isotype control (48.3±5.4%, P<0.001). Surface PD-L1 expression on TAMs was also upregulated in the combination group (MFI 2847±312 vs 1523±198, P<0.001), suggesting feedback immune activation. The proportion of tumor-infiltrating CD8$^+$ T cells increased to 28.6±3.4% in the combination group, significantly higher than in the isotype control (11.2±2.1%, P<0.001) and the anti-PD-1 monotherapy group (12.8±2.5%, P=0.001). Among combination group CD8$^+$ T cells, the proportion of IFN-γ$^+$ cells (41.3±4.8% vs 17.6±3.2%, P<0.001) and granzyme B$^+$ cells (35.7±4.1% vs 14.9±2.8%, P<0.001) were both significantly increased (Fig. 4B, Table 4B).

Figure 4

A: TAM phenotype flow

Biology and Medical Engineering
WISDOM ACADEMIC https://doi.org/10.63808/bm.v2i1.571 Volume 2 , Issue 1



B: CD8+ T cell flow

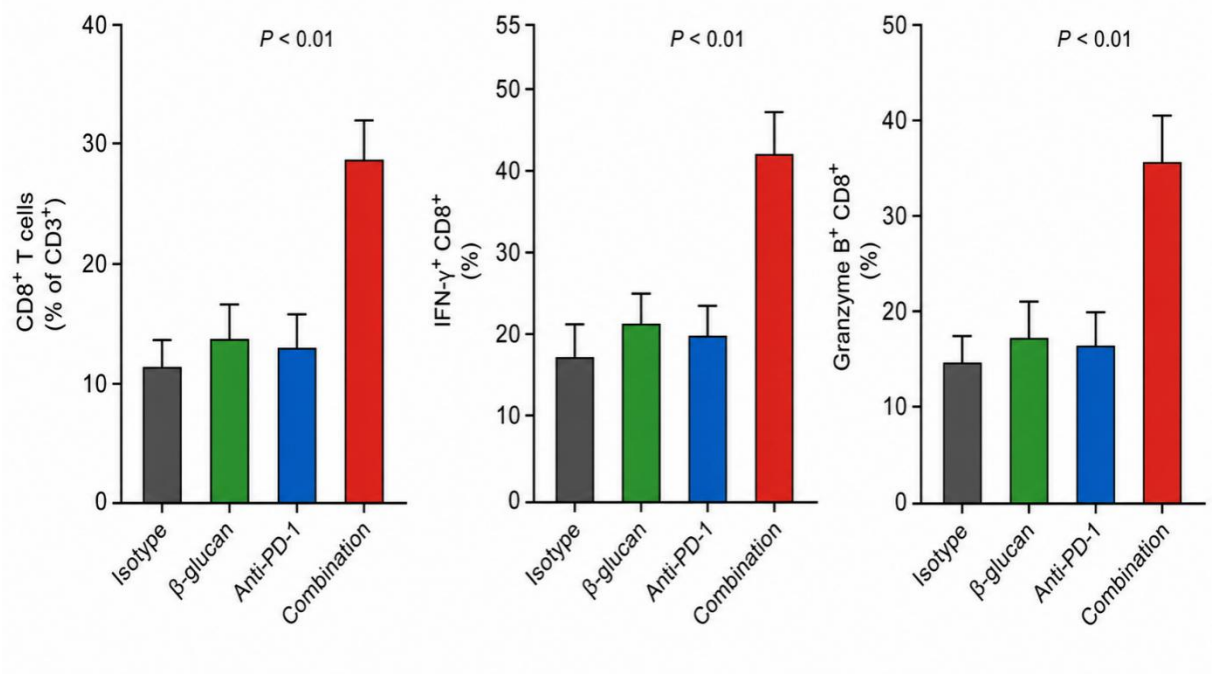


Table 4

A: TAMs phenotype flow cytometry data

Group	MHC-II⁺CD86⁺ (%)	CD206⁺Arg1⁺ (%)	PD-L1 MFI
Isotype Control	34.8±4.2	48.3±5.4	1523±198
β-Glucan	38.6±4.9	44.1±5.2	1612±224
Anti-PD-1	38.1±5.1	46.7±5.8	1587±211
Combination Group	63.4±5.7	21.7±3.9	2847±312

B: CD8⁺ T cell infiltration and function

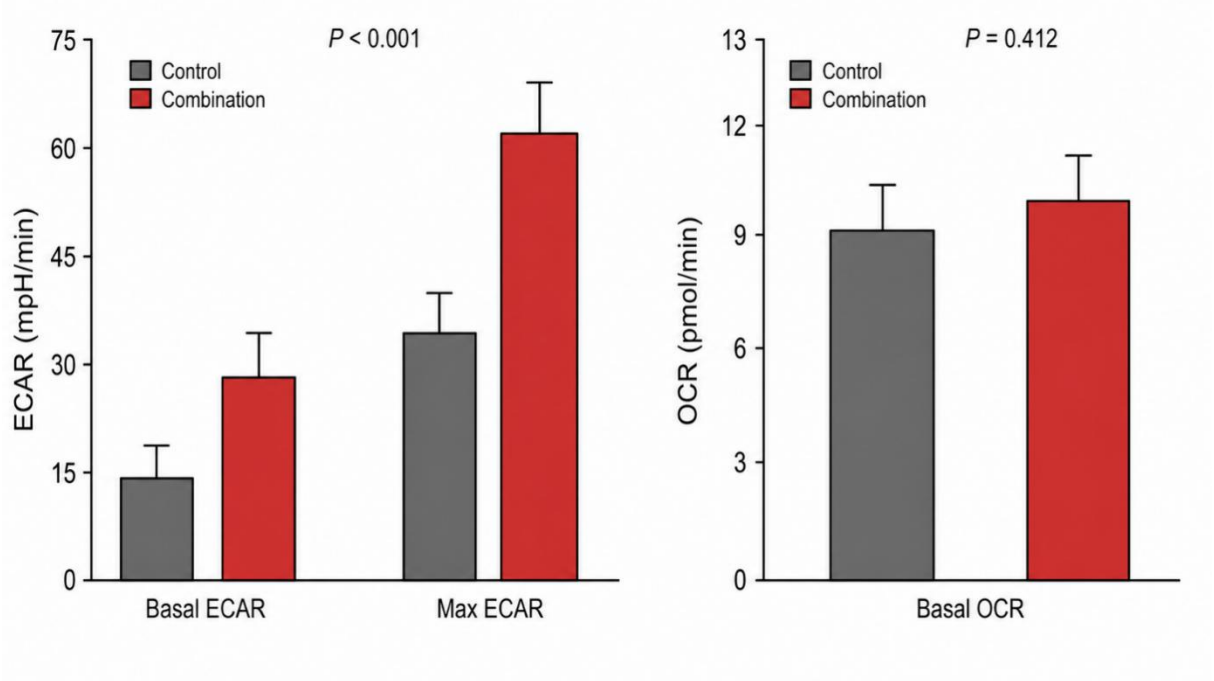
Group	$CD8^+$ as a percentage of $CD3^+$ (%)	$CD8^+$ $IFN\text{-}\gamma^+$ (%)	$CD8^+$ Granzyme B^+ (%)
Isotype Control	11.2±2.1	17.6±3.2	14.9±2.8
β-Glucan	13.5±2.4	20.4±3.6	17.2±3.1
Anti-PD-1	12.8±2.5	19.1±3.4	16.5±3.0
Combination Group	28.6±3.4	41.3±4.8	35.7±4.1

3.5. Training immune-boosting TAMs glycolysis and epigenetic reprogramming

Seahorse analysis showed that the glycolysis basal ECAR of TAMs in the combined group (28.4±3.6 mpH/min vs 14.7±2.3 mpH/min, P<0.001) and the maximum ECAR (61.2±7.1 mpH/min vs 32.5±4.8 mpH/min, P<0.001) were both significantly higher than in the control group (Fig. 5A, Table 5). There was no significant difference between the two groups in basal OCR and maximal respiration capacity (P=0.412 and P=0.367). LC-MS metabolomics showed increased levels of lactate (1.83-fold, FDR=0.006), succinate (1.52-fold, FDR=0.021), and methylglutaconate (1.71-fold, FDR=0.013) in TAMs of the combined group. ATAC-seq showed increased chromatin accessibility in the promoter regions of Tnf, Cxcl9, and H2-Ab1 in TAMs of the combined group (Fig. 5B), and ChIP-qPCR confirmed a 1.9-2.6 fold increase in H3K4me3 enrichment at these gene promoters (P<0.01; Table 5).

Figure 5

A: Seahorse ECAR OCR



B: H3K4me3 ChIP qPCR

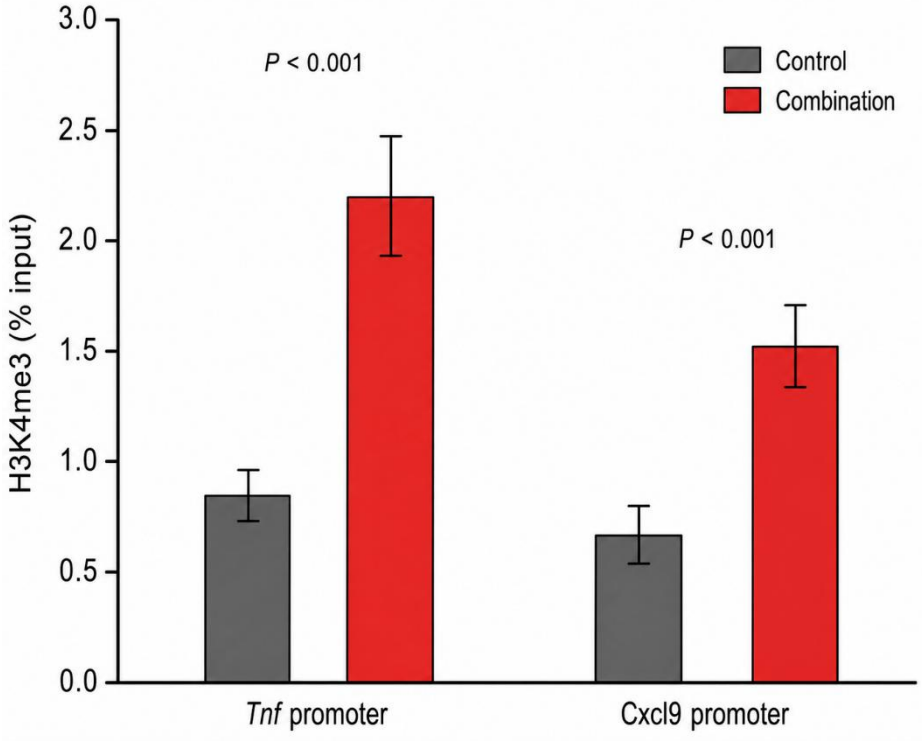


Table 5

TAMs metabolism and epigenetic reprogramming indicators

Indicators	Isotype comparison	Joint group	Multiple change	P-value
Basal ECAR (mpH/min)	14.7±2.3	28.4±3.6	1.93	<0.001
Max ECAR (mpH/min)	32.5±4.8	61.2±7.1	1.88	<0.001
Basal OCR (pmol/min)	8.9±1.4	9.6±1.5	1.08	0.412
Relative Lactic Acid Level	1.00±0.12	1.83±0.21	1.83	0.006
Relative HMG Level	1.00±0.14	1.71±0.19	1.71	0.013
Tnf Promoter H3K4me3 (% input)	0.84±0.11	2.18±0.27	2.60	<0.001
Cxcl9 Promoter H3K4me3 (% input)	0.67±0.09	1.52±0.18	2.27	<0.001

3.6. Training immune-boosted TAMs for activation of CD8⁺ T cells and antigen presentation ability

In the in vitro co-culture experiments, CD8⁺ T cells stimulated by TAMs from the combination group showed a proliferation rate (CFSE^low) of 56.8±6.2%, which was significantly higher than that of TAMs from the control group (28.4±4.1%, P<0.001; Fig. 6A). In the co-culture system with TAMs from the combination group, the proportion of CD8⁺ T cells that were IFN-γ⁺ (38.7±4.5% vs 16.2±2.9%, P<0.001) and granzyme B⁺ (31.4±3.8% vs 13.6±2.4%, P<0.001) was also significantly increased (Table 6). In the OVA-specific OT-I experiments, TAMs trained with β-glucan significantly

increased OT-I cell proliferation (62.3±6.8% vs 33.7±4.6%, P<0.001) and IFN-γ secretion (1246±187 pg/mL vs 583±94 pg/mL, P<0.001); after IFNAR1 blockade, this enhancing effect was partially reversed (proliferation 42.1±5.2%, P=0.008; IFN-γ 812±121 pg/mL, P=0.014).

Figure 6A

TAM CD8 co culture

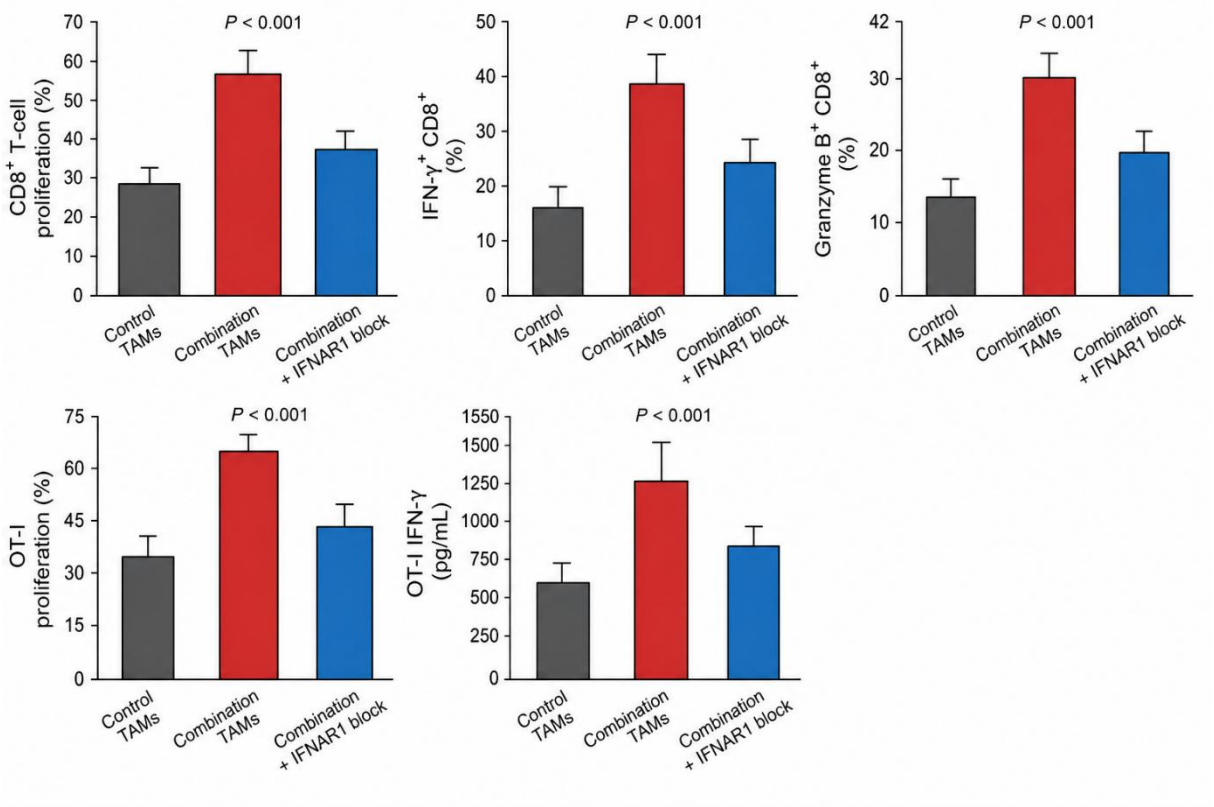


Table 6

Functional indicators of TAMs and CD8⁺ T cell co-culture

Indicators	Compare with TAMs	Joint Group TAMs	Combined IFNAR1 blockade	P value (Control vs. Combined)
CD8⁺ T cell proliferation (%)	28.4±4.1	56.8±6.2	37.2±4.8	<0.001
CD8⁺ IFN-γ⁺ (%)	16.2±2.9	38.7±4.5	24.6±3.4	<0.001
CD8⁺ Granzyme B⁺ (%)	13.6±2.4	31.4±3.8	20.1±2.9	<0.001
OT-I proliferation (%)	33.7±4.6	62.3±6.8	42.1±5.2	<0.001
OT-I IFN-γ (pg/mL)	583±94	1246±187	812±121	<0.001

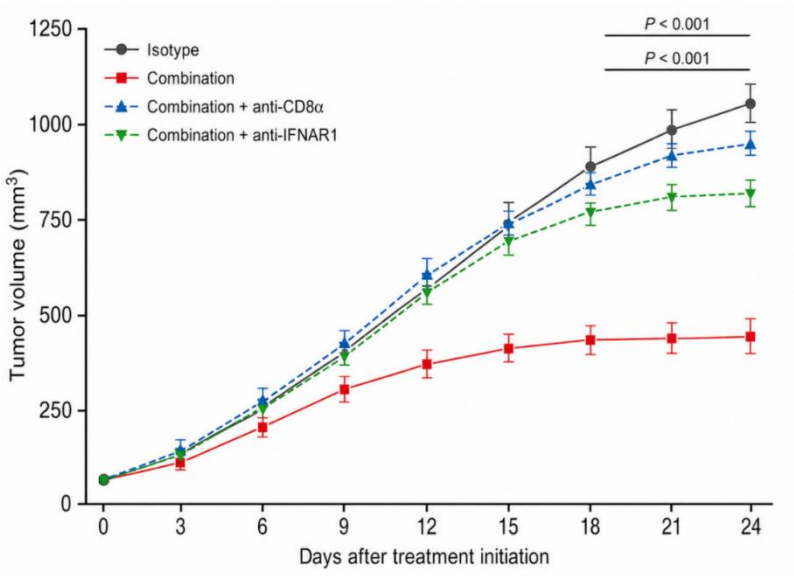
3.7. The effectiveness of combination therapy depends on CD8⁺ T cells and type I interferon signaling

To clarify the dependency of the combined therapy's effect, we removed CD8⁺ T cells or blocked

IFNAR1 on top of the combined treatment. After depleting $CD8^+$ T cells, the tumor-suppressing effect of the combination was significantly lost (Day 24 volume: Combination + anti-CD8α 958±112 mm^3 vs Combination alone 438±71 mm^3, $P<0.001$), and the median survival dropped to 31.5 days (vs Combination 52.0 days, HR=3.87, $P<0.001$; Fig. 7A, Table 7, Table 7A). After blocking IFNAR1, tumor volume in the combination group increased to 824±98 mm^3 (vs Combination $P<0.001$), and median survival decreased to 34.0 days (HR=3.12, $P<0.001$; Fig. 7B). Flow analysis showed that after IFNAR1 blockade, the proportion of TAMs that were $MHC\text{-}II^+CD86^+$ in the combination group dropped to 41.2±5.3% (vs 63.4±5.7%, $P=0.001$), and $CD8^+$ T cell infiltration decreased to 15.8±2.7% (vs 28.6±3.4%, $P<0.001$). These results indicate that the combined therapy relies on $CD8^+$ T cells and type I interferon signaling.

Figure 7

A: tumor growth dependency



B: survival dependency

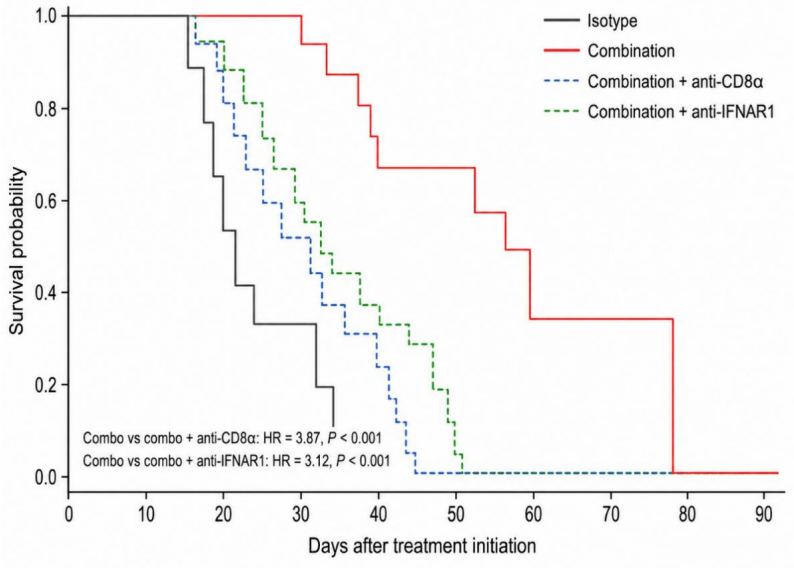


Table 7

Effects of CD8⁺ T cell depletion and IFNAR1 blockade on the efficacy of combination therapy

Groups	Tumor volume on day 24 (mm³)	Median survival (days)	TAMs MHC-II⁺CD86⁺（%）	CD8⁺ T cells as a percentage of CD3⁺
Combined Group	438±71	52.0	63.4±5.7	28.6±3.4
Combined Anti-CD8α	958±112	31.5	59.8±5.2	2.1±0.6
Combined Anti-IFNAR1	824±98	34.0	41.2±5.3	15.8±2.7
Isotype Control	1063±118	27.5	34.8±4.2	11.2±2.1

Table 7A

Tumor growth in dependency experiments (mm³, mean ± SD)

Time (d)	Isoform comparison	Joint group	Combined anti-CD8α	Combined anti-IFNAR1
0	55±9	55±9	56±10	55±9
3	128±22	110±18	132±24	126±23
6	245±42	196±31	258±44	248±42
9	389±66	295±46	412±70	392±67
12	560±92	360±56	598±98	570±94
15	735±110	405±64	742±112	704±104
18	880±116	428±69	860±116	780±104
21	990±118	435±71	930±114	815±100
24	1063±118	438±71	958±112	824±98

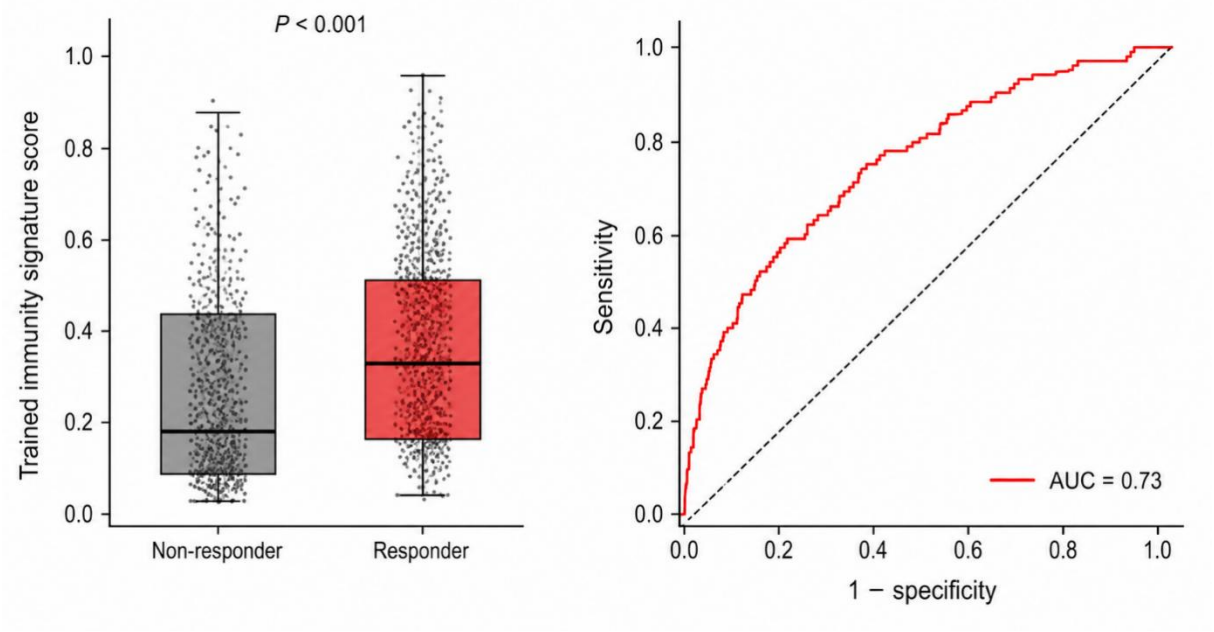
3.8. Training immune-related signatures associated with clinical ICIs response

In the IMvigor210 cohort (n=298), the trained immune signature score was significantly higher in responders to ICIs compared to non-responders (median 0.42 vs 0.18, P<0.001; Figure 8A). The ROC curve AUC was 0.71 (95% CI 0.64-0.78). The objective response rate was 38.7% in the high-score group and 17.2% in the low-score group (P<0.001). The median overall survival was not reached in the high-score group, while it was 9.8 months in the low-score group (HR=0.54, 95% CI 0.39-0.75, P<0.001; Figure 8B). In the GSE78220 cohort (n=27), responders also had significantly higher scores than non-responders (0.51 vs 0.22, P=0.012, AUC=0.76). The trained immune signature score was positively correlated with TAMs pro-inflammatory/antigen-presenting genes (CD86, CXCL9, HLA-DRA) and CD8⁺ T cell infiltration (Spearman ρ=0.48-0.61, all P<0.001), and negatively

correlated with M2-like macrophage genes (MRC1, ARG1) (ρ=-0.43, P<0.001; Table 8).

Figure 8

A: signature score and ROC



B: KM signature high vs low

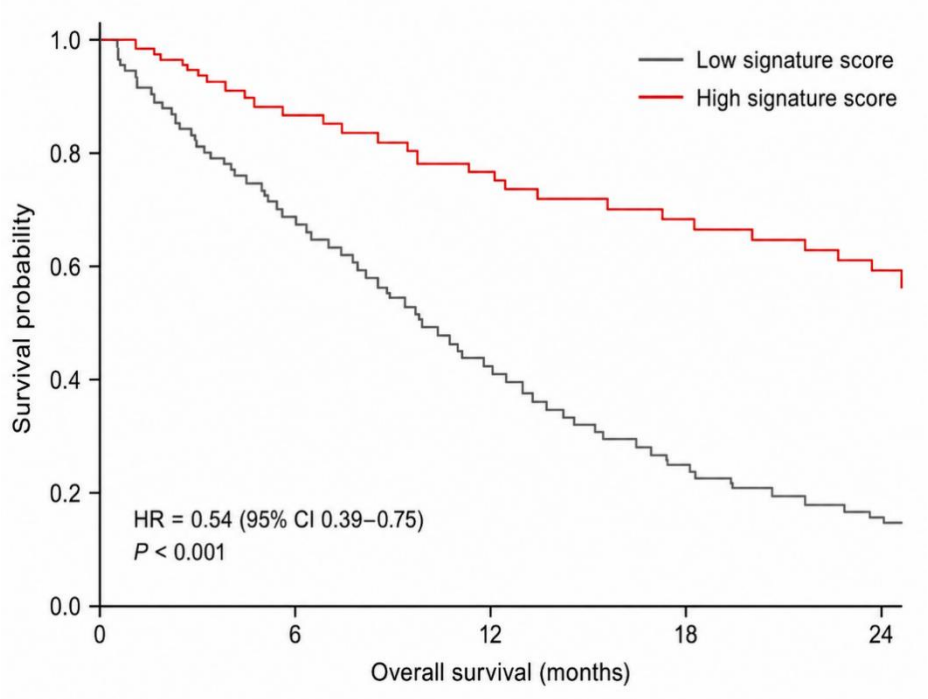


Table 8

Correlation between training immune signatures and clinical ICI responses and immune characteristics

Analysis	Queue/Metric	Result	P-value
Response vs non-response score (median)	IMvigor210	0.42 vs 0.18	<0.001

ROC AUC	IMvigor210	0.71(0.64-0.78)	—
High vs low score ORR	IMvigor210	38.7% vs 17.2%	<0.001
High vs low score OS (HR)	IMvigor210	0.54(0.39-0.75)	<0.001
Response vs non-response score	GSE78220	0.51 vs 0.22	0.012
Correlation with CD86	IMvigor210	ρ=0.61	<0.001
Correlation with CXCL9	IMvigor210	ρ=0.57	<0.001
Correlation with HLA-DRA	IMvigor210	ρ=0.48	<0.001
Correlation with MRC1	IMvigor210	ρ=-0.43	<0.001
Correlation with ARG1	IMvigor210	ρ=-0.39	<0.001

4. Discussion

This study focuses on the core question of whether trained immunity can reverse anti-PD-1 resistance by reprogramming TAMs. We established a stable MC38-R anti-PD-1 resistant model and found that β-glucan-induced trained immunity combined with anti-PD-1 can significantly suppress resistant tumor growth, extend survival, and even lead to complete remission in some mice. Mechanistically, the combination treatment prompts TAMs to shift from an M2-like immunosuppressive phenotype to a pro-inflammatory, high MHC-II antigen-presenting phenotype, accompanied by enhanced glycolysis and mevalonate pathways and increased H3K4me3 enrichment at pro-inflammatory gene promoters; the effect depends on $CD8^+$ T cells and type I interferon signaling. Analysis of clinical cohorts further showed that the trained immunity-related signature positively correlates with ICI response and survival benefits. These results connect the fields of 'innate immune training' and 'checkpoint therapy resistance,' providing a new mechanistic basis for targeting TAMs to overcome ICI resistance.

Resistance to PD-1 is a major challenge in current cancer immunotherapy, involving mechanisms like defects in antigen presentation, T cell exclusion, and an immunosuppressive tumor microenvironment (TME). TAMs contribute to resistance by secreting immunosuppressive factors, weakening antigen presentation, and promoting T cell exhaustion. Past strategies targeting TAMs mostly focused on clearing macrophages or blocking single pathways like CSF1R or CCR2. While these approaches worked in some models, they often ran into problems like compensatory recruitment of TAMs, systemic toxicity from depleting myeloid cells, and insufficient reprogramming of an already resistant TME. Unlike those approaches, this study doesn't aim to remove TAMs. Instead, it uses trained immunity to "educate" them into a new functional state, giving them long-lasting pro-inflammatory and antigen-presenting capabilities. The advantage of this strategy is that it keeps myeloid cells functioning as antigen-presenting and T cell-supporting cells while reducing their

immunosuppressive activity, making it more in line with the natural logic of immune activation.

Training immunity, as innate immune memory, is basically about boosting myeloid cell functions through epigenetic and metabolic reprogramming. Previous studies have shown that β-glucan can change the functional state of monocytes/macrophages via histone modifications like H3K4me3 and pathways like glycolysis and the mevalonate pathway. In this study, we saw similar features in tumor TAMs: after combined treatment, the glycolysis capacity and mevalonate levels of TAMs went up, and chromatin accessibility and H3K4me3 enrichment at the promoters of Tnf, Cxcl9, and H2-Ab1 increased. This suggests that trained immunity isn't just a temporary activation of TAMs—it programs them via epigenetics and metabolism to maintain a sustained pro-inflammatory memory state. Unlike previous work that mostly looked at trained immunity in vitro or in systemic myeloid cells, this study focused on training immunity specifically in TAMs within the TME and showed that their functional reprogramming is directly linked to anti-tumor effects.

Compared with existing studies on trained immunity against tumors, our findings show both continuations and differences. Kalafati and colleagues demonstrated that innate immune training at the granulopoiesis level can enhance anti-tumor activity; Priem and colleagues developed immune-training-promoting nanobiologics that can inhibit tumor growth and improve checkpoint blockade efficacy; Ding and colleagues induced trained immunity in pro-metastatic macrophages to control metastasis. These studies collectively support the therapeutic potential of trained immunity, but their interventions mostly target systemic myeloid progenitors, nanocarrier delivery, or specific macrophage subsets. Our study focuses on the clinical challenge of anti-PD-1 resistance, using a clinically translatable β-glucan pretreatment combined with anti-PD-1, and systematically shows that the efficacy depends on TAM phenotype switching, $CD8^+$ T cells, and type I interferon signaling. Notably, $CD8^+$ T cell depletion and IFNAR1 blockade almost completely abolish the benefits of the combination therapy, suggesting that trained immunity does not act solely through non-specific inflammation but requires an intact 'TAMs–type I IFN–$CD8^+$ T cell' axis. This provides direct evidence for the synergy between trained immunity and adaptive immunity and indicates that IFN-I signaling could be a key biomarker and pharmacodynamic indicator for trained immunity combined with ICIs.

We also observed PD-L1 upregulation on TAMs in the combination group. At first glance, this might suggest immune suppression, but considering the significant increase in $CD8^+$ T cell infiltration and IFN-γ production, a more reasonable explanation is IFN-I/IFN-γ-driven feedback immune activation. PD-L1 upregulation is both a result of T cell activation and may provide more binding targets for anti-PD-1 antibodies, creating a positive feedback loop. This explanation aligns with the clinical observation of dynamic PD-L1 increases in patients responding to ICIs. However, we did not directly test the impact of PD-L1 blockade in combination therapy, which should be clarified in future

studies via PD-L1 blockade or TAM-specific PD-L1 knockout.

Clinical relevance analysis provides preliminary support for the translational value of the study. In the IMvigor210 and GSE78220 cohorts, a high trained immune signature score was associated with better response to ICIs and improved survival. This signature was positively correlated with TAMs pro-inflammatory/antigen-presenting genes and $CD8^+$ T cell infiltration, and negatively correlated with M2-like genes. This aligns with previous views that trained immunity could be a potential cancer immunotherapy strategy, but this study is the first to directly link the trained immune signature with clinical ICI response and suggests it might serve as a candidate biomarker for predicting ICI efficacy. However, there are inherent limitations in analyzing public cohorts: the trained immune signature was built based on literature rather than derived from this study's data, and differences in cohort platforms and batch effects could affect score stability; IMvigor210 is a urothelial cancer cohort, and GSE78220 has a small sample size, so conclusions need validation in prospective, multi-cancer cohorts. Additionally, the independent predictive value of the signature score compared to known markers like PD-L1 expression still requires confirmation through multivariate and decision curve analysis.

This study has several limitations. It mainly relies on a single MC38-R model, which, although it consistently reproduces the PD-1 resistance phenotype, may be influenced by tumor type, mutation load, and immunogenicity, so it needs to be validated in less immunogenic models like B16-OVA and LLC, as well as in humanized mice. The source, batch, dose, and administration timing of β-glucan can significantly impact the strength of trained immunity. While our pretreatment protocol was based on previous studies, the optimal dosing window and dose-response relationship have not been systematically optimized. Sorting TAMs for in vitro co-culture may alter their phenotype and metabolic state, and the single-cell sequencing sample size was limited (3 per group), so the molecular definition and functional heterogeneity of TAM-1/TAM-2 subgroups still need larger-scale validation. IFNAR1 blockade and $CD8^+$ T cell depletion are systemic interventions, which may affect other immune cells; future studies should use conditional gene knockouts or TAM-specific interventions to clarify cell-intrinsic mechanisms. The clinical analysis is based on retrospective public data and lacks the trained immunity status of TAMs in our study cohort, their dynamic changes before and after treatment, and protein-level validation. We did not assess potential toxicity of trained immunity, such as chronic inflammation, autoimmune-like changes, or excessive activation of myeloid cells, which are crucial safety considerations for clinical translation.

Despite the limitations mentioned above, this study still has clear innovations: it is the first to show in a stable anti-PD-1-resistant tumor model that trained immunity can reverse resistance and directly link the effect to TAM phenotypes, metabolism, and epigenetic reprogramming; it clearly identifies the 'TAMs–type I interferon–$CD8^+$ T cell' axis as a key pathway for the efficacy of trained immunity combined with anti-PD-1, providing a mechanistic explanation for combination therapy; it

establishes and validates the association between trained immunity-related signatures and clinical ICI responses, offering clues for biomarker development and patient stratification; and it proposes a 'reprogramming' strategy different from TAM depletion, preserving the antigen-presenting function of myeloid cells, showing good translational potential.

Future research could focus on the following directions: optimizing the delivery methods and timing of trained immune inducers, exploring their combination with radiotherapy, chemotherapy, or other ICIs; using TAM-specific conditional knockout mice to clarify the cell-autonomous roles of type I interferon signaling and epigenetic regulators; validating trained immune signatures in human tumor samples and prospective ICI cohorts, and analyzing the spatial interactions between TAMs and $CD8^+$ T cells with spatial transcriptomics; systematically assessing the long-term safety of trained immunity and the risk of immune-related adverse events. Overall, this study provides mechanistic and translational evidence that trained immunity can reprogram TAMs to overcome anti-PD-1 resistance, suggesting that targeting innate immune memory could be a new strategy to improve ICI responses.

5. Conclusion

This study confirmed in a stable anti-PD-1 resistant tumor model that β-glucan-induced trained immunity combined with anti-PD-1 can significantly inhibit the growth of resistant tumors, extend survival, and even achieve complete remission in some mice. Mechanistically, the combination treatment reprogrammed tumor-associated myeloid cells to a pro-inflammatory, MHC-II high antigen-presenting phenotype, along with enhanced glycolysis and mevalonate pathway activity and increased H3K4me3 enrichment at pro-inflammatory gene promoters. The efficacy depended on $CD8^+$ T cells and type I interferon signaling. Clinical cohort analysis further showed that trained immunity-related signatures were positively associated with ICI response and survival benefits. These results link innate immune training with checkpoint therapy resistance, suggesting that reprogramming TAMs through trained immunity, rather than simply clearing TAMs, could be a new strategy to overcome anti-PD-1 resistance.

Future research needs to test this strategy across various low-immunogenic tumor models and humanized mice, optimize the delivery method, dose, and timing of trained immune inducers, and use TAM-specific conditional knockout models to clarify the cell-intrinsic mechanisms of type I interferon signaling and epigenetic regulators. At the same time, it's important to verify the predictive value of trained immune signatures in prospective, multi-cancer ICI cohorts, combine spatial transcriptomics to analyze the spatial interactions between TAMs and $CD8^+$ T cells, and systematically assess the long-term safety of trained immunity and the risks of immune-related adverse events. These studies could help move trained immunity combined with ICIs from mechanistic exploration to clinical translation.

Acknowledgments

Not applicable.

Author contributions

Conceptualization, Gang Liu and Jia Wang; methodology, Jia Wang; validation, Gang Liu; formal analysis, Jia Wang; investigation, Gang Liu and Jia Wang; resources, Gang Liu; data curation, Jia Wang; writing—original draft preparation, Jia Wang; writing—review and editing, Gang Liu; visualization, Jia Wang; supervision, Gang Liu; project administration, Gang Liu. All authors have read and agreed to the published version of the manuscript.

Funding

Not applicable.

Data availability

Not applicable.

Declarations

Conflict of interest

The authors declare that there is no conflict of interest.

Ethics approval

Not applicable.

Consent to participate

Not applicable.

Consent for publication

All authors have given their consent.

Additional information

Received: 9 November 2026

Accepted: 9 November 2026

Published online: 10 November 2026

Publisher's Note

Wisdom Academic Press Ltd. remains neutral with regard to jurisdictional claims in published maps and institutional affiliations.

References

[1] Bekkering, S., Arts, R. J. W., Novakovic, B., et al. (2018). Metabolic induction of trained immunity through the mevalonate pathway. *Cell, 172*(1-2), 135-146.e9. https://doi.org/10.1016/j.cell.2017.11.025

[2] Cassetta, L., & Pollard, J. W. (2018). Targeting macrophages: Therapeutic approaches in cancer. *Nat Rev Drug Discov, 17*(12), 887-904. https://doi.org/10.1038/nrd.2018.169

[3] DeNardo, D. G., & Ruffell, B. (2019). Macrophages as regulators of tumour immunity and immunotherapy. *Nat Rev Immunol, 19*(6), 369-382. https://doi.org/10.1038/s41577-019-0127-6

[4] Ding, C., Shrestha, R., Zhu, X., et al. (2023). Inducing trained immunity in pro-metastatic macrophages to control tumor metastasis. *Nat Immunol, 24*(2), 239-254. https://doi.org/10.1038/s41590-022-01388-8

[5] Gabrilovich, D. I., & Nagaraj, S. (2009). Myeloid-derived suppressor cells as regulators of the immune system. *Nat Rev Immunol, 9*(3), 162-174. https://doi.org/10.1038/nri2506

[6] Jenkins, R. W., Barbie, D. A., & Flaherty, K. T. (2018). Mechanisms of resistance to immune checkpoint inhibitors. *Br J Cancer, 118*(1), 9-16. https://doi.org/10.1038/bjc.2017.434

[7] Kalafati, L., Kourtzelis, I., Schulte-Schrepping, J., et al. (2020). Innate immune training of granulopoiesis promotes anti-tumor activity. *Cell, 183*(3), 771-785.e12. https://doi.org/10.1016/j.cell.2020.09.058

[8] Lérias, J. R., de Sousa, E., Paraschoudi, G., et al. (2020). Trained immunity for personalized cancer immunotherapy: Current knowledge and future opportunities. *Front Microbiol, 10*, 2924. https://doi.org/10.3389/fmicb.2019.02924

[9] Liu, G. (2026a). Tumor microenvironment: Composition, dynamic evolution, and its significance in cancer treatment. *Journal of Cancer Insights, 1*(1), 6. https://doi.org/10.66128/jci202601.1

[10] Liu, G. (2026b). The application of artificial intelligence in tumor immunotherapy: Integrating multi-omics data to achieve efficacy prediction and combination strategies. *Applied Artificial Intelligence Research, 2*(2). https://doi.org/10.65455/q72yq328

[11] Liu, G., & Wang, J. (2026). TOX phase separation locks T cells in a terminal exhausted state, and disrupting it can revive anti-tumor immunity. *Biology and Medical Engineering, 2*(1), 538. https://doi.org/10.63808/bm.v2i1.538

[12] Liu, G., Vasiukevich, A. M., & Wang, J. (2026f). Lactate-driven histone lactylation weakens B cell immunity in tertiary lymphoid structures. *Injury and Rehabilitation Care, 2*(1), 539. https://doi.org/10.63808/irc.v2i1.539

[13] Liu, G., Wang, J., & An, L. (2026b). CRISPR screen and single-cell multi-omics identify a novel immune checkpoint on tumor-infiltrating regulatory T cells. *Injury and Rehabilitation Care, 2*(1), 525. https://doi.org/10.63808/irc.v2i1.525

[14] Liu, G., Wang, J., & An, L. (2026c). Gut microbiota-derived butyrate induces trained immunity in intestinal macrophages to potentiate antitumor immunity. *Biology and Medical Engineering, 2*(1), 523. https://doi.org/10.63808/bm.v2i1.523

[15] Liu, G., Wang, J., & An, L. (2026e). Mitochondrial DNA sensing reshapes the tumor immune microenvironment via cooperative cGAS-STING activation and ferroptosis. *Global Health Care, 2*(1), 524. https://doi.org/10.63808/ghc.v2i1.524

[16] Liu, G., Wang, J., & Vasiukevich, A. M. (2026a). Overcoming anti-PD-1 resistance: Targeted STING activation reprograms tumor-associated macrophages. *Global Health Care, 2*(1), 540. https://doi.org/10.63808/ghc.v2i1.540

[17] Liu, G., Wang, J., & Zhu J. (2026g). Explainable spatial AI analyzes tumor-immune interactions to predict immunotherapy outcomes and identify new targets. *Intelligent & Human Futures, 2*(3), 510. https://doi.org/10.63808/ihf.v2i3.510

[18] Liu, G., Wang, J., & Zhu J. (2026h). Using multimodal foundational models to predict neoantigen immunogenicity and vaccine effectiveness across different tumor types. *Global Health Care, 2*(3), 498. https://doi.org/10.63808/ghc.v2i3.498

[19] Liu, G., Wang, J., Vasiukevich, A. M., Feng, B., & An, L. (2026d). Targeting mitochondrial metabolic reprogramming: Reversing $CD8^+$ T cell exhaustion and improving cancer immunotherapy response. *Biology and Medical Engineering, 2*(1), 531. https://doi.org/10.63808/bm.v2i1.531

[20] Mantovani, A., Marchesi, F., Malesci, A., Laghi, L., & Allavena, P. (2017). Tumour-associated macrophages as treatment targets in oncology. *Nat Rev Clin Oncol, 14*(7), 399-416. https://doi.org/10.1038/nrclinonc.2016.217

[21] Netea, M. G., Domínguez-Andrés, J., Barreiro, L. B., et al. (2020). Defining trained immunity and its role in health and disease. *Nat Rev Immunol, 20*(6), 375-388. https://doi.org/10.1038/s41577-020-0285-6

[22] Netea, M. G., Joosten, L. A., Latz, E., et al. (2016). Trained immunity: A program of innate immune memory in health and disease. *Science, 352*(6284), aaf1098. https://doi.org/10.1126/science.aaf1098

[23] Netea, M. G., Quintin, J., & van der Meer, J. W. (2011). Trained immunity: A memory for innate host defense. *Cell Host Microbe, 9*(5), 355-361. https://doi.org/10.1016/j.chom.2011.04.006

[24] Noy, R., & Pollard, J. W. (2014). Tumor-associated macrophages: From mechanisms to therapy. *Immunity, 41*(1), 49-61. https://doi.org/10.1016/j.immuni.2014.06.010

[25] Pathria, P., Louis, T. L., & Varner, J. A. (2019). Targeting tumor-associated macrophages in cancer. *Trends Immunol, 40*(4), 310-327. https://doi.org/10.1016/j.it.2019.02.003

[26] Priem, B., van Leent, M. M. T., Teunissen, A. J., et al. (2020). Trained immunity-promoting nanobiologic therapy suppresses tumor growth and potentiates checkpoint inhibition. *Cell, 183*(3), 786-801.e19. https://doi.org/10.1016/j.cell.2020.09.059

[27] Quintin, J., Saeed, S., Martens, J. H. A., et al. (2012). Candida albicans infection affords protection against reinfection via functional reprogramming of monocytes. *Cell Host Microbe, 12*(2), 223-232. https://doi.org/10.1016/j.chom.2012.06.006

[28] Riksen, N. P., & Netea, M. G. (2021). Immunometabolic control of trained immunity. *Mol Aspects Med, 77*, 100897. https://doi.org/10.1016/j.mam.2020.100897

[29] Ruffell, B., & Coussens, L. M. (2015). Macrophages and therapeutic resistance in cancer. *Cancer Cell, 27*(4), 462-472. https://doi.org/10.1016/j.ccell.2015.02.015

[30] Saeed, S., Quintin, J., Kerstens, H. H., et al. (2014). Epigenetic programming of monocyte-to-macrophage differentiation and trained innate immunity. *Science, 345*(6204), 1251086. https://doi.org/10.1126/science.1251086

[31] Sharma, P., Hu-Lieskovan, S., Wargo, J. A., & Ribas, A. (2017). Primary, adaptive, and acquired resistance to cancer immunotherapy. *Cell, 168*(4), 707-723. https://doi.org/10.1016/j.cell.2017.01.017

[32] Topalian, S. L., Drake, C. G., & Pardoll, D. M. (2015). Immune checkpoint blockade: A common denominator approach to cancer therapy. *Cancer Cell, 27*(4), 450-461. https://doi.org/10.1016/j.ccell.2015.03.001

[33] Van der Heijden, C. D. C. C., Noz, M. P., Joosten, L. A. B., Netea, M. G., Riksen, N. P., & Keating, S. T. (2018). Epigenetics and trained immunity. *Antioxid Redox Signal, 29*(11), 1023-1040. https://doi.org/10.1089/ars.2017.7310

[34] Xiang, X., Wang, J., Lu, D., & Xu, X. (2021). Targeting tumor-associated macrophages to synergize tumor immunotherapy. *Signal Transduct Target Ther, 6*(1), 75. https://doi.org/10.1038/s41392-021-00484-9